Optimal design of experiments

Oliwer Sliczniuk[a,*], Pekka Oinas[a]

[a]Aalto University, School of Chemical Engineering, Espoo, 02150, Finland

ARTICLE INFO

Keywords:
Supercritical extraction
Optimal design of experiment
Mathematical modelling
Optimization
Fisher information

ABSTRACT

This study aimed to investigate the supercritical extraction process of caraway oil from caraway seeds. The extraction was performed in a partially filled extractor with a fixed bed operated under multiple operating conditions. A distributed-parameter model describes the fluid-solid extraction process with CO_2 as a solvent. The concept of quasi-one-dimensional flow is applied to reduce the number of spatial dimensions. The flow is assumed to be uniform across any cross-section, although the area available for the fluid phase can vary along the extractor. The optimal design of experiment problem is solved to find an experimental strategy for validating the correlations between extraction kinetic parameters and the operating conditions. This work proposes two experimental strategies: one that only manipulates the inlet temperature and the second that manipulate only the pressure.

1. Introduction

The present study focuses on extracting essential oil from the caraway (Carum carvi L.) seeds with supercritical fluid extraction and modelling that process. Caraway is a biennial plant belonging to the Apiaceae family. It is widespread in Asia, Europe, and North Africa. The essential oil obtained from caraway finds its potential application as a fragrance ingredient in perfumes, liquors, and toothpaste. As presented by Hromis et al. [1], the dried caraway contains nearly 2.8–5% essential oil, from which the main compounds are carvone, pinene, camphene, limonene, and carveol.

The economic feasibility of the process is crucial when selecting the appropriate technology. Conventional processes, such as distillation and organic solvent extraction, are frequently used for essential oil extraction. The distillation process is carried out at a high temperature, which causes thermal degradation of thermolabile compounds—considering that alternative techniques like supercritical fluid extraction gained popularity for extraction. Supercritical carbon dioxide, in particular, is attractive due to its unique properties such as inflammable, non-toxic, low critical temperature and non-corrosive. Furthermore, its critical point is relatively low compared to other fluids, making it a suitable alternative to traditional extraction techniques. The supercritical fluids exhibit both gas- and liquid-like properties so that operating conditions can adjust the dissolving power.

Various mathematical models have been proposed to describe the extraction of valuable compounds from a fixed biomass bed. However, selecting an appropriate extraction model requires understanding the physical phenomena occurring in the operational unit. Each model has its own set of assumptions and describes different mass transfer mechanisms and equilibrium relationships.

One model proposed by Reverchon et al. [2] is the hot ball model, which is based on an analogy to heat transfer and describes an extraction process from solid particles containing small quantities of solute where solubility is not a limiting factor.

Another model, the Broken-and-Intact Cell model, was presented by Sovova [3]. This model describes a system where the outer surfaces of particles have been mechanically interrupted, allowing easy access of solvent to the solute from the broken cells. In contrast, the solute from the intact cells is less accessible due to high mass transfer resistance.

Reverchon [4] developed a model for fluid-solid extraction, where the oil is treated as a single component, and the extraction process is controlled by internal mass transfer resistance, neglecting external mass transfer. However, this model does not consider the influence of axial dispersion or changes in fluid density and flow rate along the bed.

In this work, the fundamental governing equations are derived and combined with the kinetic model suggested by Reverchon [4] to obtain a general model for the oil extraction process from the caraway seed. This model simplifies some of the physical behaviour to obtain a control-oriented model. It is assumed that the extraction process operates semi-continuously in a cylindrical vessel. The solvent is first brought to supercritical conditions, pumped through a fixed bed of finely chopped biomass, and the solute is extracted from the biomass. The solvent and solute are then separated in a flush drum, and the extract is collected. The feed flow rate (F_{in}) and inlet temperature (T_{in}) of the extractor can be measured and manipulated, while the vessel pressure (P) can also be measured and manipulated. However, the outlet temperature (T_{out}) can only be measured. Figure 1 shows a simplified flow diagram.

The design of experiments (DOE) also known as experiment design or experimental design, is the design of any task that aims to describe and explain the variation of information under conditions that are hypothesized to reflect the variation. The term is generally associated with experiments in which the design introduces conditions that directly affect the variation, but may also refer to the design of quasi-experiments, in which natural conditions that influence the variation are selected for observation.

*Corresponding author
oliwer.sliczniuk@aalto.fi (O. Sliczniuk)
ORCID(s): 0000-0003-2593-5956 (O. Sliczniuk); 0000-0002-0183-5558 (P. Oinas)

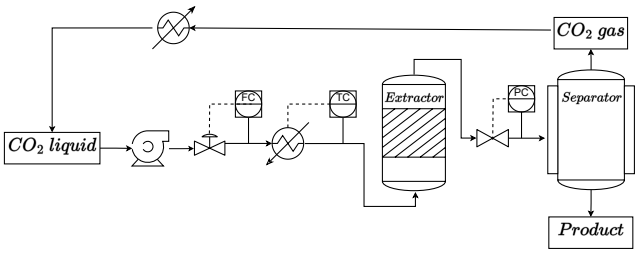

Figure 1: Process flow diagram

Oinas et al. [5] presents how the experimental design methods can be applied for analyzing mass transfer and reaction in stirred gas—liquid and gas—liquid—solid reactors. In this work a sequential approach to experimentation is suggested. First preliminary set of 8 2-level experiments (2^8 factorial design) were performed. The identifiability of the parameters was then considered and some reparametrisations done. The precision of the parameter values were further improved with D-optimal experiments.

Kassama et al. [6] used the response surface methodology with the central composite rotatetable design (CCRD) model. The goal of this work was to optimize parameters for supercritical carbon dioxide extraction of lycopene ($C_{40}H_{56}$) from dried tomato skin. The CCRD consisting of three-factored factorial design with two levels was used in this study. The factors used were temperature of the extraction chamber (40 and 70 °C), pressure of the extraction fluid (25 and 45 MPa), and modifier concentration (5 and 15%). A second-degree polynomial equation was developed from a response surface analysis for all trans-lycopene yield and the highest yield was predicted at 62 °C, 45 MPa (450 bar) and 14% temperature, pressure and modifier concentration, respectively and the recovery of all trans-lycopene was 33%.

Abrahamsson et al. [7] selected extraction conditions based on a symmetrical full factorial design of experiments with three factors and three levels. The factors were pressure ranging from 15 to 30 MPa, temperature from 313 to 353 K and compressed CO_2 pump volumetric flow rate from 0.5 to 1.5 mL/min, with three replicates at the center point (22.5 MPa, 333 K, 1 mL/min) thus resulting in a total of 29 extractions. By including all of the 29 experiments for the model calibration, a more robust estimates of parameters were obtained.

Espie and Macchietto [8] presented the case of the continuous yeast fermenter, in which a stream containing an organic substrate is fed to a well-stirred tank, and a model is sought to describe the substrate and biomass consumption. Optimal dynamic experiments are initially designed to select the best model from a set of candidate models, then to produce improved parameter estimates for the remaining model.

The study is structured as follows: Chapter 2.1 provides a general discussion on supercritical fluids to familiarize the reader with their properties. Chapter 2.2 introduces the general balance equations. The balance equations are combined with the extraction kinetic equation to develop the process model in Chapter 2.3. The general formulation of model-based the optimal design of experiments is presented in Chapter 2.4. Finally, the sensitivity plots are discussed in Chapters 3 and 4.

2. Materials and methods

2.1. Supercritical fluids

A supercritical fluid (SCF) is a substance at a temperature and pressure above its critical point, where there are no distinct liquid and gas phases but below the pressure required to compress it into a solid. SCFs can move through porous solids like gases, which is faster than liquid transport through such materials. SCFs have a higher ability to dissolve materials like liquids or solids compared to gases. Near the critical point, small changes in pressure or temperature result in significant changes in density, allowing many properties of an SCF to be fine-tuned. By changing the pressure and temperature, the properties of carbon dioxide can be tuned to be more liquid-like or gas-like.

Fluid properties can be divided into two kinds: equilibrium properties and transport properties. The equation of state can be used accurately to predict the equilibrium properties, such as fluid density, enthalpy, vapour pressure, fugacity and fugacity coefficient, vapour-liquid equilibrium, and all kinds of excess properties.

Supercritical CO_2's thermodynamic properties, such as density or specific heat capacity, vary significantly with slight changes in temperature and pressure due to real gas effects. The Peng-Robinson equation of state (P-R EOS) is used to calculate the thermodynamic properties by accounting for these real gas effects are presented in Appendix **??**. The P-R EOS belongs to a specific class of thermodynamic models for modelling the pressure of a solvent as a function of temperature and density and which can be rewritten as a cubic function of the molar volume.

To determine the thermodynamic properties of a real gas, it is necessary to evaluate the departure function of the chosen equation of state for that property. As explained by Elliott [9], the departure function describe the difference between the actual value of a thermodynamic property of a real gas and its value if the gas were ideal under the same temperature and pressure conditions. The ideal gas serves as a reference state to which the properties of real gases are compared. The departure function measures the extent to which a real gas deviates from ideal gas behaviour. The departure functions allow for the accurate calculation of thermodynamic properties for real gases.

The properties of CO_2 are presented as a function of operating conditions (temperature and pressure) in Figure 2. At standard atmospheric pressure and temperature, CO_2 behaves as an ideal gas, and its compressibility factor equals unity. However, at high pressures and/or low temperatures, intermolecular forces between gas molecules become more significant, causing them to deviate from ideal behaviour. As a result, the compressibility factor can be greater than or less than unity, depending on the magnitude of these forces. As

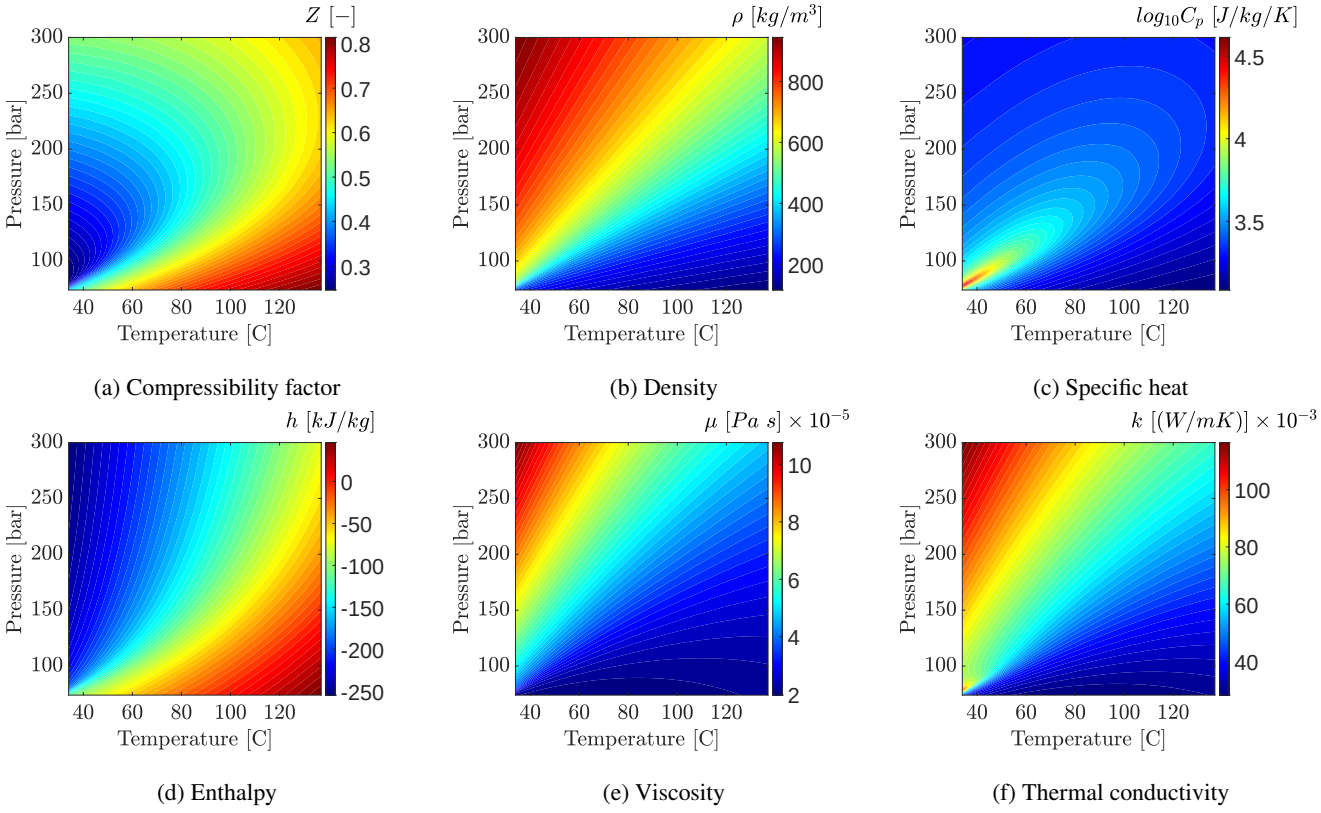

(a) Compressibility factor (b) Density (c) Specific heat

(d) Enthalpy (e) Viscosity (f) Thermal conductivity

Figure 2: Properties of CO_2 based on the equation of state and correlations

presented in Figure 2a, the compressibility factor obtained from the Peng-Robinson equation of state varies strongly depending on the operating conditions.

The real gas effects are also visible on the density plot presented in Figure 2b. The density calculations are based on the compressibility factor, and its value depends on the operating conditions. The fluid properties near the critical point are unique and combine gas-like and liquid-like properties. The details of calculations are explained in Appendix **??**.

Figure 2c show the behaviour of the heat capacity of a supercritical fluid at constant pressure (C_p). The details of the calculations can be found in Appendix **??**. Contrary to the density, which varies monotonically, the specific heat shows very high levels in a narrow region. In the subcritical region, the phase transition is associated with an effective spike in the heat capacity (i.e., the latent heat). Approaching the critical point, the latent heat falls to zero, which is accompanied by a gradual rise in heat capacity in the pure phases near phase transition. At the critical point, the latent heat is zero, but the heat capacity shows a diverging singularity. Beyond the critical point, there is no divergence, but rather a peak in the heat capacity; the highest point of this peak identifies the Widom line (as discussed by Simeoni et al. [10] and Banuti [11]).

Figure 2d represent how the specific enthalpy change with the operating conditions. The details of calculations are discussed in Appendix **??**.

Transport properties such as viscosity and conductivity play a crucial role in engineering design for production, fluid transportation, and processing. However, as highlighted by Sheng et al. [12], developing a satisfactory theory for transport properties of real dense gases and liquids is a challenging task. This is due to the inherent difficulties involved in accurate measurements and the complexity involved in theoretical treatments.

To address this issue, the correlations of transport coefficients are either empirical or based on some theoretical foundation. Chapman-Enskog's theory (presented in Chapman and Cowling [13]) for transport properties of dense gases based on the distribution function is a popular theoretical approach. However, the Chapman-Enskog theory was developed for rigid spherical molecules and modifications are required to apply it to real gases. Many correlations have been proposed following the Chapman-Enskog theory in the form of reduced density and reduced temperature, such as those developed by Fenghour et al. [14], and Laesecke and Muzny [15] from the National Institute of Standards and Technology (NIST). The correlation of Laesecke and Muzny [15] is presented in Figure 2e.

NIST has developed a viscosity formulation consisting of four contributions: (i) for the limit of zero density, (ii) for the initial density dependence, (iii) for the residual viscosity, and (iv) for the singularity of the viscosity at the critical point. The NIST correlation covers temperatures from 100 to 2000 K for gaseous CO_2, and from 220 to 700 K with

pressures along the melting line up to 8000 MPa for compressed and supercritical liquid states. These correlations and theories are essential in predicting transport properties for real gases and liquids and can assist in engineering design and analysis.

Similarly, the NIST developed the correlation, which describe the behaviour of thermal diffusivity of CO_2. The work of Huber et al. [16] captures the singular behaviour of thermal conductivity around the critical point. The correlation is applicable for the temperature range from the triple point to 1100 K and pressures up to 200 MPa. Figure 2f shows how the thermal conductivity of carbon dioxide change depending on the operating conditions.

2.2. Governing equations

The governing equation for a quasi-one-dimensional compressible flow in Cartesian coordinates can be found in the Appendix **??** and in the work of Anderson [17]. Quasi-one-dimensional flow is a fluid flow characterized by the assumption that the flow properties remain uniform across any given cross-section of the flow. This assumption is made when there is a variation in the cross-sectional area of the flow channel, such as an irregular shape or partial filling of an extractor. In such cases, the flow is considered to be quasi-one-dimensional because the velocity and other flow properties are assumed to vary only in the direction of flow.

The quasi-one-dimensional compressible Navier-Stokes equations in Cartesian coordinates are given by Equations 1 to 3. The derivation of these Equations are presented in Appendix **??**.

$$\frac{\partial\left(\rho_f A_f(z)\right)}{\partial t}+\frac{\partial\left(\rho_f A_f(z) v\right)}{\partial z}=0 \tag{1}$$

$$\frac{\partial\left(\rho_f v A_f(z)\right)}{\partial t}+\frac{\partial\left(\rho_f A_f(z) v^2\right)}{\partial z}=-A_f(z)\frac{\partial P}{\partial z} \tag{2}$$

$$\frac{\partial\left(\rho_f e A_f(z)\right)}{\partial t}+\frac{\partial\left(\rho_f A_f(z) v e\right)}{\partial z}=-P\frac{\left(A_f(z) v\right)}{\partial z}+\frac{\partial}{\partial z}\left(\frac{\partial T}{\partial z}\right) \tag{3}$$

where ρ_f is the density of the fluid, $A_f(z)$ is the function which describe change of the cross-section, v is the velocity, P is the total pressure, e is the internal energy of the fluid, t is time and z is the spacial direction.

Based on governing equations, the small discontinuity (defined as δ) in flow properties, shown in Figure 3, can be analysed. The analysis follows the work of Schreier [18].

	ρ_f	$\rho_f+\delta\rho_f$	
$v\rightarrow$	P	$P+\delta P$	$v+\delta v\rightarrow$
	T	$T+\delta T$	

Figure 3: Small discontinuity in one-dimensional flow

The discontinuity is presumed to be at rest relative, and the balance equations become

$$\rho_f\delta v+v\delta\rho_f+\delta\rho_f\delta v=0$$
$$\delta P=\delta v\delta\rho_f$$

These relations are equally valid if the two regions are separated by a region of finite width rather than a discontinuity.

$$\lim_{\rho_f v\rightarrow 0}\rho_f\delta v+v\delta\rho_f+\delta\rho_f\delta v=0/\delta\rho_f\rightarrow\frac{dv}{d\rho_f}=-\frac{v}{\rho_f}$$

By combining the momentum equation with the above equation, we get

$$\frac{dv}{d\rho_f}=-\frac{dv}{dP}\frac{dP}{d\rho_f}=-\frac{1}{\rho v}\frac{dP}{d\rho_f}=-\frac{v}{\rho_f} \tag{4}$$

Suppose the flow is presumed to be isentropic, $dP/d\rho_f = c^2$, so $v^2 = c^2$, where c is the speed of sound. This can be interpreted as a small pressure wave propagating with the speed of sound relative to the flow. Moreover, if the flow velocity is relatively low, all pressure changes are hydrodynamic (due to velocity motion) rather than thermodynamic which leads to $\partial\rho_f/\partial P \approx 0$. In other words, the small changes in pressure due to flow velocity changes do not change the density.

2.3. Extraction model

2.3.1. Continuity equation

The obtained above quasi-one-dimensional continuity equation (Equation 1) is further modified by specifying a function $A_f(z) = A\phi(z)$ to take into account the change of the cross-section available for the fluid. The Equation 5 shows the differential form of the continuity equation:

$$\frac{\partial(\rho_f(T(t,z),P(t))\phi(z))}{\partial t}+\frac{\partial(\rho_f(T(t,z),P(t))v A\phi(z))}{\partial z}=0 \tag{5}$$

where A is the total cross-section of the extractor and $\phi(z)$ describe porosity along the extractor.

Assuming that the mass flow rate is constant in time, the temporal derivative becomes zero, and the spatial derivative can be integrated along z as

$$\int\frac{\partial(\rho_f(T(t,z),P(t))v A\phi(z))}{\partial z}dz=0\rightarrow F=\rho_f(T(t,z),P(t))v A\phi(z) \tag{6}$$

Here, F is a constant obtained from the integration and is understood as the mass flux per unit area, which is assumed to be constant along z. To simplify the dynamics of the system, it is assumed that $F = F(t)$ is a control variable and affects the whole system instantaneously. This assumption allows for finding the velocity profile that satisfies mass continuity based on $F(t)$, $\phi(z)$, and $\rho_f(T(t,z),P(t))$.

$$v=\frac{F(t)}{\rho_f(T(t,z),P(t))A\phi(z)} \tag{7}$$

The fluid density $\rho_f(T(t,z),P(t))$ can be obtained from an equation of state if temperature and the thermodynamic pressure (assumed $P(t)$ to be constant along z due to the low-Mach number condition) are known. The variation in density may be caused by the fluid accumulation in the system (equivalent to pressure change), which occurs instantaneously along z or by a temperature change.

Analogously, the superficial velocity might be introduced to the model and defined as

$$u=v\phi(z)=\frac{F(t)}{\rho_f(T(t,z),P(t))A} \tag{8}$$

2.3.2. Mass balance for the fluid phase

The detailed derivation of the mass balance equation for the fluid phase can be found in Appendix **??**. The movement of the pseudo-homogeneous fluid phase (Equation 9) is considered only in the axial direction due to quasi-one-dimensional assumptions, which take into account variation of the void fraction. Furthermore, the thermodynamic pressure is assumed to be constant along the device as presented by Equation 4. Additionally, the boundary layer adjacent to the inner wall of the extractor is neglected, resulting in a constant velocity profile across any cross-section of the extractor perpendicular to the axial direction. The amount of solute in the solvent is considered negligible, resulting in the fluid phase being described as pseudo-homogeneous, and its properties are assumed to be the same as the solvent. The mass balance equation for the fluid phase includes convection, diffusion, and kinetic terms.

$$\frac{\partial c_f(t,z)}{\partial t}+\frac{1}{\phi(z)}\frac{\partial\left(c_f(t,z)u\right)}{\partial z}=\frac{1-\phi(z)}{\phi(z)}r_e(t,z)+\frac{1}{\phi(z)}\frac{\partial}{\partial z}\left(D_e^M\frac{\partial c_f(t,z)}{\partial z}\right) \tag{9}$$

$c_f(t,z)$ represents the concentration of solute in the fluid phase, , $r_e(t,z)$ is a mass transfer kinetic term, and $D_e^M(T(t,z),P(t),F(t))$ is the axial mass diffusion coefficient.

2.3.3. Mass balance for the solid phase

The solid phase is considered to be stationary, with negligible convection and diffusion terms in the mass balance equation (Equation 10). Therefore, the only significant term in this equation is the kinetic term (as defined in Equation 11), which connects the solid and fluid phases. The extract is represented by a single pseudo-component to simplify the analysis.

$$\frac{\partial c_s(t,z)}{\partial t}=\underbrace{r_e(t,z)}_{\text{Kinetics}} \tag{10}$$

2.3.4. Kinetic term

The kinetic term in this study is based on the two-film theory proposed by Reverchon [4], and the mass transfer kinetic is given by Equation 11. This equation takes into account the overall diffusion coefficient and the concentration gradient, which acts as the driving force for the process.

As the solvent flows through the bed, CO_2 molecules diffuse into the pores and adsorb on the particle surface to form an external fluid film around the solid particles due to the solvent-solid matrix interactions. The effect of Knudsen diffusion is negligible in this process, as the mean free path of the molecule is much smaller than the pore diameter. The dissolved solute diffuses from the particle's core through the solid-fluid interface, the pore, and the film into the bulk. Figure 4 illustrates the mass transfer mechanism, where the mean solute concentration in the solid phase is denoted as c_s and the equilibrium concentrations at the solid-fluid interface are denoted as c_s^* and c_p^*, respectively, for solid and fluid phases. The concentration of the solutes in the fluid phase in the center of the pore is denoted as c_p. As the solute diffuses through the pore, its concentration changes and reaches c_{pf} at the opening of the pore. The solute then diffuses through the film around the particle and reaches a concentration in bulk c_f. The two-film theory describes the solid-fluid interface inside the pore. The overall mass transfer coefficient can be determined if the relationship between the solute concentration in one phase and its equilibrium concentration is known.

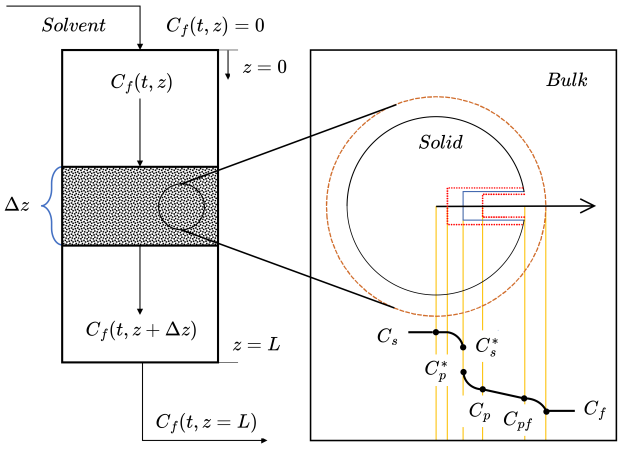

Figure 4: The extraction mechanism

Bulley et al. [19] suggests a process where the driving force for extraction is given by the difference between the concentration of the solute in bulk, c_f, and in the center of the pore, c_p^*. The concentration c_p^* is in equilibrium with c_s according to an equilibrium relationship. The rate of extraction is thus $r_e\left(c_f-c_p^*(c_s)\right)$.

On the other hand, Reverchon [4] proposes a driving force given by the difference between c_s and c_p^*. c_p^* is determined by an equilibrium relationship with c_f and the extraction rate is $r_e\left(c_s-c_p^*(c_f)\right)$ or more precisely

$$r_e(t,z)=\frac{D_i(T(t,z),P(t))}{\mu l^2}\left(c_s(t,z)-c_P^*(t,z)\right) \tag{11}$$

where μ is sphericity, l a characteristic dimension of particles and can be defined as $l=r/3$, r is the mean particle radius, ρ_s is the solid density, $D_i(T(t,z))$ corresponds to the overall diffusion coefficient and $c_P^*(t,z)$ is a concentration at the solid-fluid interface (which according to the internal resistance model is supposed to be at equilibrium with the fluid phase).

According to Bulley et al. [19], a linear equilibrium relationship (equation 12) can be used to find an equilibrium concentration of the solute in the fluid phase $c_f^*(t,z)$ is based on the concentration of the solute in the solid phase $c_s(t,z)$

$$c(t,z)=k_p(T(t,z),P(t))q^*(t,z) \tag{12}$$

The volumetric partition coefficient $k_p(T(t,z),P(t))$ behaves as an equilibrium constant between the solute concentration in one phase and the corresponding equilibrium

concentration at the solid-fluid interphase. According to Spiro and Kandiah [20], the term $k_p(T(t,z),P(t))$ can be expressed as the function of mass partition factor $k_m(T(t,z))$.

$$k_m(T(t,z)) = \frac{k_p(T(t,z),P(t))\rho_s}{\rho(T(t,z),P(t))} \tag{13}$$

Equation 14 represents of the kinetic term according to Reverchon [4]

$$r_e(t,z) = -\frac{D_i(T(t,z),P(t))}{\mu l^2}\left(c_s(t,z) - \frac{\rho_s}{k_m(T(t,z))\rho_f(T(t,z),P(t))}c_f(t,z)\right) \tag{14}$$

2.3.5. *Uneven distribution of the solute in the solid phase*

Following the idea of the Broken-and-Intact Cell (BIC) model presented by Sovova [21], the internal diffusion coefficient D_i is consider to be a product of the reference value of D_i^R and the exponential decay function γ, as given by Equation 15.

$$D_i = D_i^R\gamma(c_s(t,z)) = D_i^R\exp\left(\Upsilon\left(1-\frac{c_s(t,z)}{c_{s0}}\right)\right) \tag{15}$$

where the Υ describe the curvature of the decay function. The final form of the extraction kinetic Equation is given by Equation 16.

$$r_e(t,z) = -\frac{D_i^R(T(t,z),P(t))\gamma(c_s(t,z))}{\mu l^2}\left(c_s(t,z) - \frac{\rho_s}{k_m(T(t,z))\rho(T(t,z),P(t))}c_f(t,z)\right) \tag{16}$$

Such a formulation limits the availability of the solute in the solid phase. Similarly to the BIC model, if solute is assumed to be contained in the cells, a part of which is open because the cell walls were broken by grinding, and the rest remains intact. The diffusion of the solute from a particle's core takes more time compared to the diffusion of the solute located close to the outer surface. Considering that the internal diffusion coefficient decay as the concentration of the solute in the solid decrease. As the value of the c_s decrease over time, the exponential term approach unity and $\lim_{c_s\to 0} D_i = D_i^R$. D_i^R can be interpreted as the internal diffusion coefficient at vanishing gradient.

Alternatively, the decay function γ can be consider with respect to the Shrinking Core model presented by Goto et al. [22], where the particle radius change as the amount of solute in the solid phase decrease. As the particle size decrease due to dissolution, the diffusion path increase which makes the diffusion slower and reduce the value of a diffusion coefficient. The same analogy can be apply to the Equation 15 to explain the change of the diffusion coefficient.

2.3.6. *Heat balance*

The heat governing equation describe the evolution of the energy in the system and it is given by 17. The derivation of the heat equation can be found in Appendix **??**.

$$\frac{\partial\left(\rho_f(T(t,z),P(t))e(t,z)A_f\right)}{\partial t} + \frac{\partial\left(\rho_f(T(t,z),P(t))A_f v e(t,z)\right)}{\partial z} = -P(t)\frac{\left(A_f v\right)}{\partial z} + \frac{\partial}{\partial z}\left(\frac{\partial T(t,z)}{\partial z}\right) \tag{17}$$

The departure function is a mathematical function that characterizes the deviation of a thermodynamic property (enthalpy, entropy, and internal energy) of a real substance from that of an ideal gas at the same temperature and pressure. The departure function is typically defined as the difference between the value of a thermodynamic property for a real fluid and the corresponding value for an ideal gas at the same temperature and pressure. They are typically computed by integrating a function that depends on the equation of state and its derivatives. Following Elliott [9] or Gmehling et al. [23], a real gas internal energy definition can be obtained from the departure functions, defined through Equation 18. More information on the departure functions can be found in Appendix **??**.

$$de(t,z) = C_v dT - \left[P(t) - T(t,z)\left(\frac{\partial P(t)}{\partial T(t,z)}\right)_{v_m(T(t,z),P(t))}\right]dv_m(T(t,z),P(t)) \tag{18}$$

where $e^{id}(t,z)$ is the internal energy of perfect gas.

Suppose a gas is considered to be perfectly caloric ($e(t,z) = C_v T(t,z)$), then the energy equation can be written explicitly in the form of temperature. The perfectly caloric gas can be seen as the special case of a real gas, where the second term of Equation 18 goes to zero and the heat capacity C_v is constant.

For real gases, it is complicated to write the heat balance in terms of temperature, but it be can be used directly in the form of internal energy, as it is given by Equation 3. In such a case, the temperature needs to be recovered from the internal energy. A relation for the internal energy can be obtained from an equation of state. For Peng-Robinson, such a relation is given by Equation 19 as presented by Elliott [9].

$$\frac{e(t,z)-e^{id}(t,z)}{RT(t,z)} = -\frac{A(T(t,z),P(t))}{B(T(t,z),P(t))\sqrt{8}}\frac{\kappa\sqrt{T_r}}{\sqrt{\alpha}}\ln\left[\frac{Z(T(t,z),P(t)) + \left(1+\sqrt{2}\right)B(T(t,z),P(t))}{Z(T(t,z),P(t)) + \left(1-\sqrt{2}\right)B(T(t,z),P(t))}\right] \tag{19}$$

To solve Equation 19, temperature, pressure, and density values need to be known. If an equation of state is introduced, then only two out of three variables need to be obtained as the third one can be calculated; this can be represented as follow

$$e(t,z) = e(T(t,z),P(t),\rho_f(T(t,z),P(t))) = e(T(t,z),P(t),\rho_f(T(t,z),P(t))) \tag{20}$$

If the value of internal energy $e(t,z)$ is known from the time evolution of the energy Equation 3, and pressure is known from measurement, then the temperature can be reconstructed. A roootfinder can be used to find a value of temperature, which minimizes the difference between the value of internal energy coming from the time evolution

(Equation 17) and the output from Equation 19. Such a procedure allow to find local temperature along spatial direction z and needs to be repeated every time-step.

Another way to express the energy equation is to introduce enthalpy $h(t,z) = e(t,z) + P(t)/\rho_f(T(t,z),P(t))$. By introducing the definition of enthalpy, the energy equation becomes

$$\frac{\partial\left(\rho_f(T(t,z),P(t))h(t,z)A_f\right)}{\partial t} - \frac{\partial\left(P(t)A_f\right)}{\partial t} + \frac{\partial\left(\rho_f(T(t,z),P(t))h(t,z)A_f v\right)}{\partial z} - \frac{\partial}{\partial z}\left(k\frac{\partial T(t,z)}{\partial z}\right) \tag{21}$$

The main advantage of this formulation is the presence of term $\partial P(t)/\partial t$, which allows it to directly affect the system through the change of thermodynamic pressure (which is a control variable). The enthalpy is related to the pressure and temperature through the following equation:

$$h(t,z) = h(T(t,z),P(t),\rho_f(T(t,z),P(t))) = h(T(t,z),P(t),\rho_f(T(t,z),P(t))) \tag{22}$$

If the value of enthalpy is known from the time evolution and pressure can be measured, then the Equation 22 can be solved for the temperature to recover the temperature profile. For the Peng-Robinson EoS, the enthalpy can be defined by Equation 23. More details can be found in Appendix **??** or given by Gmehling et al. [23].

$$h(t,z) - h(t,z)^{id} = RT(t,z)\left[T_r(Z(T(t,z),P(t)) - 1) - 2.078(1+\kappa)\sqrt{\alpha(T(t,z))}\ln\left(\frac{Z(T(t,z),P(t)) + \left(1+\sqrt{2}\right)B(T(t,z),P(t))}{Z(T(t,z),P(t)) + \left(1-\sqrt{2}\right)B(T(t,z),P(t))}\right)\right] \tag{23}$$

The Equation 23 requires an reference sate, which in this case is assumed to be $T_{ref} = 298.15\ [K]$ and $P_{ref} = 1.01325\ [bar]$.

As discussed by Gmehling et al. [23], the influence of the intermolecular forces on the enthalpy is needs to taken into account in high pressures systems. In most cases, these forces are attractive, so additional energy is necessary to move the molecules away from each other, that is, to lower the density. If this energy is not added, the substance cools down when it is expanded.

2.3.7. Pressure term

The pressure term in the energy equation, given by Equation 21, describes the change of the thermodynamic pressure with respect to time. As explained in Chapters 2.2, at Low-Mach number conditions, the thermodynamic pressure is nearly constant in space due to the small pressure wave propagation that occurs at the speed of sound. Under such conditions, the term $\partial P/\partial t$ can be approximated by an ordinary differential equation, which describes the instantaneous change of pressure in the system. The pressure (P) in the system is considered a state variable, while the pressure in the new time-step (P_{in}) is considered a control variable.

$$\frac{\partial P(t)}{\partial t} \approx \frac{P(t) - P_{in}(t)}{\Delta t} \tag{24}$$

Such a simplified equation takes into account the pressure change in the energy balance, but the dynamics are simplified and do not consider the effects of pressure losses. In a real system, the dynamics of pressure change would depend on a pump used in an extraction system, as well as a back-pressure regulator used to control an outlet valve.

2.3.8. Extraction yield

The efficiency of the process (the yield) is calculated according to Equation 25 as presented by Sovova et al. [24]. The measurement equation evaluate the mass of solute at the outlet of the extraction unit and sums it. The integral form of the measurement equation (25) can be transformed into the differential form (26) and augmented with the process model.

$$y(t) = \int_{t_0}^{t_f} \frac{F(t)}{\rho_f(T(t,z),P(t))} c_f(t,z)\Big|_{z=L} dt \tag{25}$$

$$\frac{dy(t)}{dt} = g(x(t)) = \frac{F(t)}{\rho_f(T(t,z),P(t))} c_f(t,z)\Big|_{z=L} \tag{26}$$

2.3.9. Initial and boundary conditions

It is assumed that the solvent is free of solute at the entrance of the extractor and that all the solid particles have the same initial solute content c_{s0}. Every SFE system needs some time to reach the desired operating conditions but the solute diffuses from solid phase to the fluid phase already at the preparation stage. For instance, a pump introduce more fluid to the extractor to increase the pressure, which makes the fluid present already in that vessel to moves internally hence the solute in the fluid phase is non-uniformly distributed. Some conclusions can be drawn from the analysis of the initial part of each yield curve obtained from the laboratory (Figure **??**). It can be noticed that each curve at the beginning has a non-linear curvature. A quadratic function could approximate the initial part of each extraction curve. A function that, after integration, gives a quadratic-like result is a straight line. Based on that observation, the solute concentration in the fluid phase is assumed to be linearly distributed. The solute concentration is assumed to be zero at the outlet and reach the maximum at the beginning of the fixed bed. The details on the calculation are given in Appendix **??**. The linear distribution $H(z)$ can be defined if the total mass of solute m_{total} and initial mass ratio between solid and fluid phases τ are known. Moreover, it is considered that the initial temperature of the extractor in every place is the same and described by h_0. Therefore, the initial conditions employed in the simulation are:

$$c_f(t=0,z) = H(z) \quad c_s(t=0,z) = c_{s0} \quad h(t=0,z) = h_0$$

2.3.10. State-space representation

The process model can be written in a general form:

$$\begin{bmatrix} \frac{\partial c_f(t,z)}{\partial t} \\ \frac{\partial c_s(t,z)}{\partial t} \\ \frac{\partial h(t,z)}{\partial t} \\ \frac{\partial P(t,z)}{\partial t} \\ \frac{\partial y(t)}{\partial t} \end{bmatrix} = \begin{bmatrix} \bar{\phi}_1\left(c_f(t,z),c_s(t,z),h(t,z);\Theta\right) \\ \bar{\phi}_2\left(c_f(t,z),c_s(t,z),h(t,z);\Theta\right) \\ \bar{\phi}_3\left(c_f(t,z),c_s(t,z),h(t,z);\Theta\right) \\ \bar{\phi}_4\left(c_f(t,z),c_s(t,z),h(t,z);\Theta\right) \\ \bar{\phi}_5\left(c_f(t,z),c_s(t,z),h(t,z);\Theta\right) \end{bmatrix} = \bar{\phi}(t,z;\Theta) = \frac{\partial \chi(t,z)}{\partial t} \tag{27}$$

where Θ is a paramter space, $\bar{\phi}$ is a set of functions that correspond to state equations of the model, and χ is the state-space model.

Function $\bar{\phi}$ are transformed to a corresponding set of N_z discretized equations denoted as G. The state-space model $\chi(t, z)$ after the discretization is represented by $\dot{x}(t)$.

$$\dot{x}(t) = \frac{dx(t)}{dt} = \begin{bmatrix} \frac{dc_{f,1}(t)}{dt} \\ \vdots \\ \frac{dc_{f,N_z}(t)}{dt} \\ \hline \frac{dc_{s,1}(t)}{dt} \\ \vdots \\ \frac{dc_{s,N_z}(t)}{dt} \\ \hline \frac{dh_1(t)}{dt} \\ \vdots \\ \frac{dh_{N_z}(t)}{dt} \\ \hline \frac{dP(t)}{dt} \\ \hline \frac{dy(t)}{dt} \end{bmatrix} = \underbrace{\begin{bmatrix} G_1\left(c_f(t), c_s(t), h(t); \Theta\right) \\ \vdots \\ G_{N_z}\left(c_f(t), c_s(t), h(t); \Theta\right) \\ \hline G_{N_z+1}\left(c_f(t), c_s(t), h(t); \Theta\right) \\ \vdots \\ G_{2N_z}\left(c(t), c_s(t), h(t); \Theta\right) \\ \hline G_{2N_z+1}\left(c_f(t), c_s(t), h(t); \Theta\right) \\ \vdots \\ G_{3N_z}\left(c_f(t), c_s(t), h(t); \Theta\right) \\ \hline G_{3N_z+1}\left(c_f(t), c_s(t), h(t); \Theta\right) \\ \hline G_{3N_z+2}\left(c_f(t), c_s(t), h(t); \Theta\right) \end{bmatrix}}_{G(x(t);\Theta)}$$

where $x \in \mathbb{R}^{N_x=3N_z}$ and $\Theta \in \mathbb{R}^{N_\Theta=N_\theta+N_u}$, N_θ is the number of model parameters, N_u is the number of control variables.

In a state-space sense, the state variables of the system are the local concentrations of solute in the fluid and solid phases ($c_f(t, z)$ and $c_s(t, z)$, respectively), and the local enthalpy of the pseudo-homogeneous phase ($h(t, z)$). The controllable input variables are the mass flow-rate and temperature of the solvent in the feed and the pressure in the extractor. Additionally, the pressure change is augmented with the state-space and denoted as $P(t)$. The system state-space is extended by assuming that extraction yield can be modelled as a function of a known initial mass of solute in the solid phase and it can be measured after the separator ($Y(t)$). The system is controllable by manipulating the flow-rate and temperature (enthalpy) of CO_2 in the feed, and the pressure in the extractor.

2.3.11. Discretization methods

The method of lines is used to transform the process model equations into a set of ODEs denoted as $G(x(t); \Theta)$. The partial derivatives in z-direction are computed using a first-order and second-order finite difference approximation. The backward finite difference is used to approximate the first-order derivative, while the central difference scheme is used to approximate the second-order derivative. The length of the fixed bed is divided into N_z equally distributed points in z-direction.

As presented in Appendix **??**, all the governing can be written in the integral form using the Divergence Theorem. The integral equation states that the change rate of the integral of any quantity over an arbitrary control volume is given by the flux through the boundary of the control volume, with being the outer surface normal through the boundary. That quantity is neither produced nor consumed inside of the control volume and is hence conserved. For a derivative to be conservative, it must form a telescoping series. In other words, after the addition of all terms coming from the discretization over a grid, only the boundary terms should remain and the artificial interior points should cancel out. To ensure the mass conservation, the discretization is applied on the conservative form of the process model.

2.4. Design of experiment

2.4.1. Maximum likelihood

Following the work of Walter and Pronzato [25], the vector $\hat{p}_{ml}$ will be a maximum-likelihood estimate if it maximizes the cost function:

$$j_{ml}(p) = \pi_y(Y|p) \tag{28}$$

If p were fixed, $\pi_y(Y|p)$ would be the probability density of the random vector Y generated by a model with parameters p and observations Y. Considered as a function of p, $\pi_y(Y|p)$ is then called the likelihood of Y. The maximum-likelihood method looks for the parameter vector p value that gives the observed data the highest likelihood. In practice, it is often easier to look for $\hat{p}_{ml}$ by maximizing the log-likelihood function, yielding the same estimate since the logarithm function is monotonically increasing.

$$j_{ml}(p) = \ln(\pi_y(Y|p)) \tag{29}$$

Assume that the observed outputs satisfy

$$Y(t_i) = y(t_i, p^*) + \epsilon_i, \qquad i = 1, ..., n_t \tag{30}$$

where the vector $y(t_i, p^*)$ is the output of a deterministic model, p^* is the true value of the parameter vector, and the error ϵ_i belongs to a sequence of independent random variables with probability density $\pi_\epsilon(\epsilon_i)$. Since the ϵ_i are independent

$$\pi_\epsilon(\epsilon_1, \epsilon_2, ..., \epsilon_{n_t}) = \prod_{i=1}^{n_t} \pi_{\epsilon_i}(\epsilon_i) \tag{31}$$

Consider the output error

$$e^y(t_i, p) = Y(t_i) - y(t_i, p) \tag{32}$$

For the true value of the parameters, it satisfies $e^y(t_i, p^*) = \epsilon_i$. and, since y is deterministic, $\pi_{y_i}(Y(t_i)|p) = \pi_{\epsilon_i}(e^y(t_i), p)$. The likelihood of the n_t observations can be written as

$$\pi_y(Y|p) = \prod_{i=1}^{n_t} \pi_{\epsilon_i}(e^y(t_i, p)) = \prod_{i=1}^{n_t} \pi_{\epsilon_i}(Y(t_i) - y(t_i, p)) \tag{33}$$

If the noise is assumed to follow the normal distribution with the standard deviation σ, which is known from the parameter estimation:

$$\pi_y(Y|p) = \prod_{i=1}^{n_t} \frac{1}{\sqrt{2\pi\sigma_{t_i}^2}} \exp\left(-\frac{1}{2}\left(\frac{Y(t_i) - y(t_i,p)}{\sigma_{t_i}}\right)^2\right) \tag{34}$$

The associated log-likelihood can be written as

$$\ln(\pi_y(Y|p)) = (\text{term independent of p}) - \frac{1}{2}\sum_{i=1}^{n_t}\left(\frac{Y(t_i) - y(t_i,p)}{\sigma_{t_i}}\right)^2 \tag{35}$$

Its gradient is thus

$$\frac{\partial}{\partial p}\ln(\pi_y(Y|p)) = \sum_{i=1}^{n_t}\left[\left(\frac{Y(t_i) - y(t_i,p)}{\sigma_{t_i}^2}\right)\frac{\partial y(t_i,p)}{\partial p}\right] \tag{36}$$

2.4.2. Fisher information

The Fisher information is a way of measuring the amount of information that an observable random variable carries about an unknown parameter of a distribution that models the random variable. The Fisher information is related to the second derivative (or the curvature) of the log-likelihood function with respect to the parameter. This relationship provides a measure of how "sensitive" the likelihood is to changes in the parameter value. The Fisher information matrix can be calculated as follow.

$$\begin{aligned}
\mathcal{F}(p) &= -\mathop{\mathbb{E}}_{Y|p}\left[\frac{\partial^2 \ln(\pi_y(Y|p))}{\partial p \partial p^\top}\right] = \mathop{\mathbb{E}}_{Y|p}\left[\frac{\partial \ln(\pi_y(Y|p))}{\partial p}\frac{\partial \ln(\pi_y(Y|p))}{\partial p^\top}\right] \\
&= \mathop{\mathbb{E}}_{Y|p}\left[\sum_{k=1}^{n_t}\left(\frac{Y(t_k) - y(t_k,p)}{\sigma_{t_k}^2}\frac{\partial y(t_k,p)}{\partial p}\right)\times\sum_{i=1}^{n_t}\left(\frac{Y(t_i) - y(t_i,p)}{\sigma_{t_i}^2}\frac{\partial y(t_i,p)}{\partial p^\top}\right)\right] \\
&= \mathop{\mathbb{E}}_{Y|p}\left[\sum_{k=1}^{n_t}\sum_{i=1}^{n_t}\left[\left(\frac{Y(t_k) - y(t_k,p)}{\sigma_{t_k}^2}\frac{\partial y(t_k,p)}{\partial p}\right)\times\left(\frac{Y(t_i) - y(t_i,p)}{\sigma_{t_i}^2}\frac{\partial y(t_i,p)}{\partial p^\top}\right)\right]\right] \\
&= \sum_{k=1}^{n_t}\sum_{i=1}^{n_t}\mathop{\mathbb{E}}_{Y|p}\left[\left(\frac{Y(t_k) - y(t_k,p)}{\sigma_{t_k}^2}\frac{\partial y(t_k,p)}{\partial p}\right)\times\left(\frac{Y(t_i) - y(t_i,p)}{\sigma_{t_i}^2}\frac{\partial y(t_i,p)}{\partial p^\top}\right)\right] \\
&= \sum_{k=1}^{n_t}\sum_{i=1}^{n_t}\frac{1}{\sigma_{t_k}^2}\frac{\partial y(t_k,p)}{\partial p}\frac{1}{\sigma_{t_i}^2}\frac{\partial y(t_i,p)}{\partial p^\top}\mathop{\mathbb{E}}_{Y|p}\left[\left(Y(t_k) - y(t_k,p)\right)\times\left(Y(t_i) - y(t_i,p)\right)\right]
\end{aligned}$$

Considering the mismatch between the dataset and the model output, the Equation 32 can be used too redefine the expectation $\mathbb{E}_{Y|p}$ as $\mathbb{E}_{Y|p}\left[\left(Y(t_i) - y(t_i,p)\right)\left(Y(t_k) - y(t_k,p)\right)\right] = \mathbb{E}_{Y|p}\left[\epsilon_i\epsilon_k\right]$. For $i = k$, the expectation of ϵ_i is the variance of the noise $\sigma_{t_i}^2$. Analogously, the expectation becomes 0 if $i \neq k$ because the measurement noises are independent at different times.

$$\mathop{\mathbb{E}}_{Y|p}\left[\left(Y(t_i) - y(t_k,p)\right)\left(Y(t_i) - y(t_i,p)\right)\right] = \sigma_{t_i}^2\delta_{ik} \tag{37}$$

where δ_{ik} represents the Kronecker delta. Given the property of the Kronecker delta, the double summation in the Fisher Information matrix reduces to a single summation:

$$\mathcal{F}(p) = \sum_{i=1}^{n_t}\left(\frac{1}{\sigma_{t_i}^2}\frac{\partial y(t_i,p)}{\partial p}\frac{\partial y(t_i,p)}{\partial p^\top}\right) \tag{38}$$

If every experiment at time t_i is independent and characterized by its own σ_{t_i}, then the Fisher information matrix can be presented in the more compact way:

$$\mathcal{F}(p) = \frac{\partial y(t,p)}{\partial p}\begin{bmatrix}\frac{1}{\sigma_{t_1}^2} & 0 & 0\\ 0 & \ddots & 0\\ 0 & 0 & \frac{1}{\sigma_{t_{n_t}}^2}\end{bmatrix}\frac{\partial y(t,p)}{\partial p^\top} \tag{39}$$

2.4.3. Cramer-Rao inequality

Let $\hat{p}$ be an (absolutely) unbiased estimator p^*, i.e. such that it were possible to replicate the same experiment and estimate $\hat{p}$ an infinite number of times, the mean of the estimates would coincide with the true value. Let Σ be the covariance matrix of this estimator. Since $\hat{p}$ is unbiased, Σ can be written as

$$\Sigma = \mathop{\mathbb{E}}_{Y|p^*}\left[\left(\hat{p}(Y) - p^*\right)\left(\hat{p}(Y) - p^*\right)^\top\right] \tag{40}$$

which quantifies how the estimates are spread around the true value p^*. One would like the estimates to be as concentrated as possible around this true value. An estimator $\hat{p}_1$ with covariance matrix Σ_1 is said to be more efficient than an estimator $\hat{p}_2$ with covariance matrix Σ_2 if $\Sigma_1 < \Sigma_2$, that is if $\Sigma_2 - \Sigma_1$ is positive-definite (i.e.if all the eigenvalues of $\Sigma_2 - \Sigma_1$ arc strictly positive). Since estimators with high efficiency are desirable, a natural request is to make P as small as possible. The Cramer-Rao inequality provides a lower bound to what can be achieved.

Under the hypotheses that:

- the set of all data vectors Y with $\pi_y(Y|p) > 0$ does not depend on p
- $\frac{\partial \pi_y(Y|p)}{\partial p_i}\ \left(i = 1, 2, ..., n_p\right)$ is absolutely integrable
- $\mathbb{E}_{Y|p}\left[\frac{\partial \ln(\pi_y(Y|p))}{\partial p}\frac{\partial \ln(\pi_y(Y|p))}{\partial p^\top}\right]$ exists and is invertible

the covariance of any absolutely unbiased estimator satisfies

$$\Sigma \geq \mathcal{F}^{-1}(p^*) \tag{41}$$

In other words, the precision to which we can estimate p is limited by the Fisher information of the likelihood function. Based on the Cramer-Rao inequality, the Fisher information matrix can used to calculate the covariance matrices associated with maximum-likelihood estimates.

2.4.4. Optimal experimental design

The optimal design of experiments (DOE) is a statistical concept that refers to the process of planning an experiment, which allow parameters to be estimated without bias and with minimum variance. Optimal design ensures that the experiment can provide the most informative data possible. This often involves balancing the study of main effects and interactions between factors. Moreover, by efficiently planning experiments, optimal design aims to reduce the overall resources required, such as time, materials, and manpower.

The methodology for data to estimate the parameters of a specific model is influenced by a series of qualitative decisions made throughout the experimental and modelling process, such as: a model structure, a location of sensors or an equipment. Once these choices have been made, the experimenter still has some freedom to specify the quantitative experimental conditions (such as temperature, pressure, sampling times, etc.). Experiment design aims to determine

experimental conditions adapted to the final purpose of the modeling.

Let's consider that each scalar observation in a study can be expressed as $y(\xi_i)$, where the n_ξ-dimensional vector ξ_i representing the specific experimental conditions (such as the timing of measurements, operating conditions, etc.) under which the i'th observation is gathered. When collecting n_t such observations, the assembly of these ξ_i vectors forms the matrix $\Xi = (\xi_1, \xi_2, ..., \xi_{n_t})$, which combine all the experimental conditions that need optimization. In order to align the design of the experiment with practical realities, it's important to take into account various constraints, such as the total duration of the experiments, the maximum temperature of the inlet stream, and the minimum interval between sampling events. The set of all possible combinations for $\bar{\Xi}$ that adhere to these constraints is denoted as Ξ.

The formulation of a cost function j allows for the framing of optimal experiment design as a problem of constrained optimization. In this context, the optimal experiment, denoted as Ξ^*:

$$\Xi^* = \arg \underset{\Xi \in \bar{\Xi}}{\text{opt}}\ j(\Xi) \tag{42}$$

The cost function should describe the amount of information from an experiment. For that purpose it can be assumed a function κ can be related to the Fisher information obtained an arbitrary operating conditions.

$$j(\Xi) = \kappa\left[\mathcal{F}(p, \Xi)\right] \tag{43}$$

A general class of optimality criteria for DOE is given by

$$\begin{aligned} \kappa_k(\mathcal{F}(p)) &= \left[\frac{1}{n_p}\text{trace}\left(Q\mathcal{F}^{-1}(p,\Xi)Q^\top\right)^k\right]^{1/k} && \text{if det } \mathcal{F} \neq 0 \\ \kappa_k(\mathcal{F}(p)) &= \infty && \text{if det } \mathcal{F} = 0 \end{aligned} \tag{44}$$

where Q is a weighting matrix. The special case $k = 1$ corresponds to the L-optimality cost function,

$$j_L(\Xi) = \text{trace}\left[Q^\top Q\mathcal{F}^{-1}(p,\Xi)\right] \tag{45}$$

and choosing $Q = \mathbf{I}_{n_p}$ then corresponds to the A-optimality cost function. An A-optimal experiment minimizes the sum of the squares of the lengths or the axes of asymptotic confidence ellipsoids. Choosing Q diagonal, with $[Q]_{ii} = 1/p_i$ corresponds to C-optimality, which is connected with the relative precision of estimates. Taking Q to be a row vector leads to c-optimality. Taking $Q = \mathbf{I}_{n_p}$ and $k = \infty$ corresponds to E-optimality; E-optimal design maximizes the smallest eigenvalues of the Fisher information matrix and thus minimizes the length of the largest axis of the asymptotic confidence ellipsoids. The most widely used optimality criterion has $k = 0$, $Q = \mathbf{I}_{n_p}$, requiring minimization of $\det \mathcal{F}^{-1}(p, \Xi)$, or, equivalently, maximization of

$$j_D(\Xi) = \det \mathcal{F}(p, \Xi) \tag{46}$$

A D-optimal experiment minimizes the volume of the asymptotic confidence ellipsoids for the parameters. The graphical representation of the different optimality conditions is shown in Figure 5.

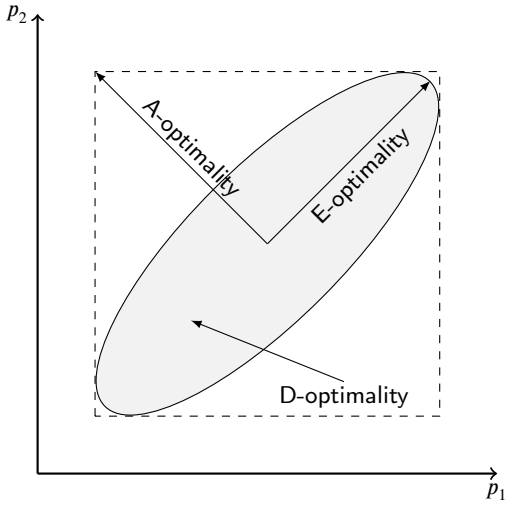

Figure 5: Graphical representation of score functions

2.4.5. Problem formulation

The optimal design of experiments technique is used to extend the experimental procedure discussed in (*article* 1), where supercritical extraction from caraway seeds has been discussed. The presented extraction was performed under multiple operating conditions, such that the temperature, pressure, and flow rate were constant during each batch. Later, the experiments' results are combined, and correlations for extraction kinetic parameters are presented. In this work, the optimal design of the experiment is used to design an experiment to validate these correlations. The Fisher information is computed with respect to correlations for D_i and Υ, which gives in total fours parameters. The model parameters, the extraction time (150 minutes), and the sampling time (5 minutes) are the same as in (*article* 1) to mimic the original system. It is assumed that the flow rate is constant because the effect of the flow rate has not been deeply investigated in the previous work of the authors (*articl* 1). In this work, two cases are considered.

In the first one, the initial temperature (T^0) of the extractor and the inlet temperature (T^{in}) are decision variables in the optimization. At the same time, the pressure is assumed to be constant during the whole experiment. It is considered that the initial state is isothermal, so $T^0 = T^{in}(t = 0)$. The inlet temperature is changed every 5 minutes and is considered constant inside this time period (piecewise constant controls). The residence time in the extractor is approximately 20-25 minutes (depending on the operating conditions). It is assumed that there is no change in the inlet temperature in the last 25 minutes of extraction, so the extractor becomes isothermal at the end of the experiment. The lower ($40°C$) and upper ($50°C$) bounds for the temperature are limits of the previous experiments (*article* 1). The general formulation of the optimal design of the experiment problem is presented below.

$$
\begin{aligned}
\Xi^* &= \arg \min_{T^0, T^{in} \in \Xi} \int_{t_0}^{t_f} -\ln j_D(\Xi, y(g(x(t)))) dt \\
\text{subject to} \quad & \\
& \dot{x} = G(x, t, \theta; \Xi) \\
& \dot{y} = g(x(t)) \\
& 40°C \leq T^{in}(t) \leq 50°C \\
& P(t) = 250\text{bar} \\
& T^0 = T^{in}(t = 0) \\
& t_0 = 0\ [min] \\
& t_f = 150\ [min]
\end{aligned} \tag{47}
$$

The second experiment strategy uses pressure as the decision variable. Contrary to the previous cases, the pressure change affects the temperature inside the extractor. It is expected to observe the heat front propagation along the system if the inlet temperature is kept at a constant value (for example, using a heat exchanger). Such a configuration leads to a more complex system response than in the first case. In contrary to the real system, the model assumes instantaneous pressure change. Depressurization in experimental systems is a rapid process, and such a simplification is acceptable. The pressure build-up is a slower process than the depressurization and requires more effort from the experimenter. To take it into account, it is assumed that the pressure can be changed less frequently than the inlet temperature in the previous case. The model parameters, the extraction time (150 minutes) and the sampling time (5 minutes), stay the same, but the pressure changes every 15 minutes (compared to 5 minutes in the first case). Initially, the extractor is kept at a constant temperature of $45°C$, which is in the middle of the previously investigated domain. The inlet temperature is also kept at $45°C$. The state constraints are included to ensure the pressure manipulation does not move the extractor temperature outside the confidence interval. The pressure can be manipulated in the range from 200 bar to 300 bar. The general formulation of the optimal design of the experiment problem is presented below.

$$
\begin{aligned}
\Xi^* &= \arg \min_{P \in \Xi} \int_{t_0}^{t_f} -\ln j_D(\Xi, y(g(x(t)))) dt \\
\text{subject to} \quad & \\
& \dot{x} = G(x, t, \theta; \Xi) \\
& \dot{y} = g(x(t)) \\
& 200\text{bar} \leq P(t) \leq 300\text{bar} \\
& 40°C \leq T(t, x) \leq 50°C \\
& T^{in} = 45°C \\
& t_0 = 0\ [min] \\
& t_f = 150\ [min]
\end{aligned} \tag{48}
$$

3. Results

Both non-linear optimization problems are solved by applying a single-shooting technique to obtain the trajectory under the assumption of piece-wise constant controls. The CasADi framework is used as the interface for the IPOPT solver. Each simulation problem is solved multiple times, starting from different initial points, and the solution with the best score is considered the optimal solution.

The first optimization problem was solved 69 times, starting from random initial guesses for the inlet temperature profile. The initial and final values of the objective function for each optimization are presented in Figure 6. It can be observed that multiple local minima are presented in the Figure. The global solution is selected from all the local solutions as the smallest local minima.

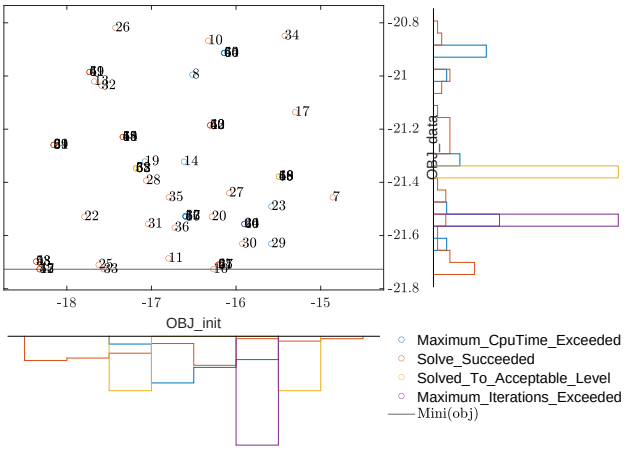

Figure 6: Solution to the first DOE

The inlet temperature profile, which corresponds to the solution of the first optimization problem, is presented in Figure 7a. The general shape of the inlet temperature profile is similar to a square wave, with the second wave being wider than the first. The maximum and the minimum values correspond to the upper and the lower constraints for the inlet temperature. The similarity with a bang-bang controller should be mentioned, although the second wave has two intermediate values between the bounds.

Figure 7b shows the temperature profile at outlet of the extractor. The outlet profile differs from the inlet profile due to heat diffusion.

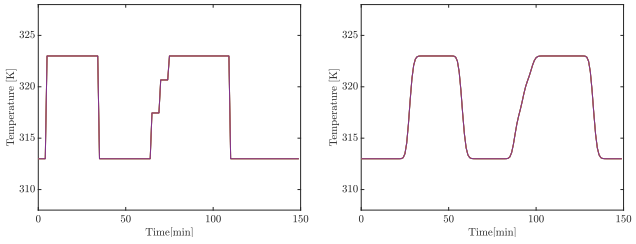

(a) Inlet temperature profile (b) Outlet temperature profile

Figure 7: Global solution to the first optimization problem

4. Conclusions

References

[1] Nevena M. Hromis, Vera L. Lazic, Sinisa L. Markov, Zuzana G. Vastag, Senka Z. Popovic, Danijela Z. Suput, Natalija R. Dzinic, Aleksandra S. Velicanski, and Ljiljana M. Popovic. Optimization of chitosan biofilm properties by addition of caraway essential oil and beeswax. Journal of Food Engineering, 158:86–93, aug 2015. doi: 10.1016/j.jfoodeng.2015.01.001.

[2] Ernesto Reverchon, Giorgio Donsi, and Libero Sesti Osseo. Modeling of supercritical fluid extraction from herbaceous matrices. Industrial & Engineering Chemistry Research, 32(11):2721–2726, nov 1993. doi: 10.1021/ie00023a039.

[3] H. Sovova. Rate of the vegetable oil extraction with supercritical co2. modelling of extraction curves. Chemical Engineering Science, 49 (3):409–414, 1994. doi: 10.1016/0009-2509(94)87012-8.

[4] E. Reverchon. Mathematical modeling of supercritical extraction of sage oil. AIChE Journal, 42(6):1765–1771, June 1996. ISSN 1547-5905. doi: 10.1002/aic.690420627.

[5] P. Oinas, I. Turunen, and H. Haario. Experimental design with steady-state and dynamic models of multiphase reactors. Chemical Engineering Science, 47(13–14):3689–3696, September 1992. ISSN 0009-2509. doi: 10.1016/0009-2509(92)85086-q.

[6] Lamin S. Kassama, John Shi, and Gauri S. Mittal. Optimization of supercritical fluid extraction of lycopene from tomato skin with central composite rotatable design model. Separation and Purification Technology, 60(3):278–284, May 2008. ISSN 1383-5866. doi: 10.1016/j.seppur.2007.09.005.

[7] Victor Abrahamsson, Niklas Andersson, Bernt Nilsson, and Charlotta Turner. Method development in inverse modeling applied to supercritical fluid extraction of lipids. The Journal of Supercritical Fluids, 111:14–27, May 2016. ISSN 0896-8446. doi: 10.1016/j.supflu.2016.01.006.

[8] D. Espie and S. Macchietto. The optimal design of dynamic experiments. AIChE Journal, 35(2):223–229, February 1989. ISSN 1547-5905. doi: 10.1002/aic.690350206.

[9] J Elliott. Introductory chemical engineering thermodynamics. Prentice Hall, Upper Saddle River, NJ, 2011. ISBN 9780136068549.

[10] G. G. Simeoni, T. Bryk, F. A. Gorelli, M. Krisch, G. Ruocco, M. Santoro, and T. Scopigno. The widom line as the crossover between liquid-like and gas-like behaviour in supercritical fluids. Nature Physics, 6(7):503–507, jun 2010. doi: 10.1038/nphys1683.

[11] Daniel Banuti. The latent heat of supercritical fluids. Periodica Polytechnica Chemical Engineering, 63(2):270–275, jan 2019. doi: 10.3311/ppch.12871.

[12] W. Sheng, G. J. Chen, and H. C. Lu. Prediction of transport properties of dense gases and liquids by the peng-robinson (PR) equation of state. International Journal of Thermophysics, 10(1):133–144, jan 1989. doi: 10.1007/bf00500714.

[13] Sydney Chapman and T. G. Cowling. The Mathematical Theory of Non-uniform Gases. Cambridge University Press, 1991. ISBN 9780521408448.

[14] A. Fenghour, William A. Wakeham, and V. Vesovic. The viscosity of carbon dioxide. Journal of Physical and Chemical Reference Data, 27 (1):31–44, jan 1998. doi: 10.1063/1.556013.

[15] Arno Laesecke and Chris D. Muzny. Reference correlation for the viscosity of carbon dioxide. Journal of Physical and Chemical Reference Data, 46(1):013107, mar 2017. doi: 10.1063/1.4977429.

[16] M. L. Huber, E. A. Sykioti, M. J. Assael, and R. A. Perkins. Reference correlation of the thermal conductivity of carbon dioxide from the triple point to 1100 k and up to 200 MPa. Journal of Physical and Chemical Reference Data, 45(1):013102, mar 2016. doi: 10.1063/1.4940892.

[17] John D. Anderson. Computational fluid dynamics the basic with applications. McGraw-Hill, 1995. ISBN 9780071132107.

[18] Stefan Schreier. Compressible flow. Wiley, 1982. ISBN 047105691X.

[19] N. R. Bulley, M. Fattori, A. Meisen, and L. Moyls. Supercritical fluid extraction of vegetable oil seeds. Journal of the American Oil Chemists' Society, 61(8):1362–1365, aug 1984. doi: 10.1007/bf02542243.

[20] M. Spiro and M. Kandiah. Extraction of ginger rhizome: partition constants and other equilibrium properties in organic solvents and in supercritical carbon dioxide. International Journal of Food Science & Technology, 25(5):566–575, jun 2007. doi: 10.1111/j.1365-2621.1990.tb01116.x.

[21] Helena Sovova. Broken-and-intact cell model for supercritical fluid extraction: Its origin and limits. The Journal of Supercritical Fluids, 129:3–8, nov 2017. doi: 10.1016/j.supflu.2017.02.014.

[22] Motonobu Goto, Bhupesh C. Roy, and Tsutomu Hirose. Shrinking-core leaching model for supercritical-fluid extraction. The Journal of Supercritical Fluids, 9(2):128–133, jun 1996. doi: 10.1016/s0896-8446(96)90009-1.

[23] Jürgen Gmehling, Michael Kleiber, Bärbel Kolbe, and Jürgen Rarey. Chemical Thermodynamics for Process Simulation. Wiley, mar 2019. doi: 10.1002/9783527809479.

[24] H. Sovova, R. Komers, J. Kucuera, and J. Jezu. Supercritical carbon dioxide extraction of caraway essential oil. Chemical Engineering Science, 49(15):2499–2505, aug 1994. doi: 10.1016/0009-2509(94)e0058-x.

[25] Eric Walter and Luc Pronzato. Identification of parametric models from experimental data. Communications and control engineering. Springer [u.a.], London, [repr.] edition, 2010. ISBN 9781849969963. Bibliography: p381 - 403. - Includes index.